Formation of Chlorinated Organic Compounds from Cl Atom-Initiated Reactions of Aromatics and Their Detection in Suburban Shanghai

Chuang Li[1], Lei Yao[1,2]*, Yuwei Wang[1], Mingliang Fang[1], Xiaojia Chen[1], Lihong Wang[1], Yueyang Li[1], Gan Yang[1], Lin Wang [1,2,3,4,5]*

[1] Shanghai Key Laboratory of Atmospheric Particle Pollution and Prevention (LAP[3]), Department of Environmental Science and Engineering, Jiangwan Campus, Fudan University, Shanghai 200438, China

[2] Shanghai Institute of Pollution Control and Ecological Security, Shanghai 200092, China

[3] IRDR International Center of Excellence on Risk Interconnectivity and Governance on Weather/Climate Extremes Impact and Public Health, Fudan University, Shanghai 200438, China

[4] National Observations and Research Station for Wetland Ecosystems of the Yangtze Estuary, Shanghai, 200433, China

[5] Collaborative Innovation Center of Climate Change, Nanjing, 210023, China

Corresponding Author: L.Y., email, lei_yao@fudan.edu.cn; phone, +86-21-31243568

L.W., email, lin_wang@fudan.edu.cn; phone, +86-21-31243568

Abstract. Chlorine (Cl) atoms generated from the photolysis of atmospheric reactive chlorine species can rapidly react with various volatile organic compounds (VOCs), forming chlorine- and non-chlorine-containing low-volatile oxygenated organic molecules. Yet, the formation mechanisms of chlorine-containing oxygenated organic molecules (Cl-OOMs) from reactions of Cl atoms with aromatics in the presence and absence of NO_x are not fully understood. Here, we investigated Cl-OOMs formation from Cl-initiated reactions of three typical aromatics (i.e., toluene, m-xylene, and 1,2,4-trimethylbenzene (1,2,4-TMB)) in the laboratory and searched for ambient gaseous Cl-OOMs in suburban Shanghai. From our laboratory experiments, 19 Cl-containing peroxyl radicals and a series of Cl-OOMs originating from the Cl-addition-initiated reaction were detected, which provides direct evidence that the Cl-addition-initiated reaction is a non-negligible pathway. In addition, a total of 51 gaseous Cl-OOMs were identified during the winter in suburban Shanghai, 38 of which were also observed in laboratory experiments, hinting that Cl-initiated reaction of aromatics could serve as a source of Cl-OOMs in an anthropogenically influenced atmosphere. Toxicity evaluation of these Cl-

OOMs shows potential adverse health effects. These findings demonstrate that Cl-OOMs can be efficiently formed via the Cl-addition pathway in the reactions between aromatics and Cl atoms and some of these Cl-OOMs could be toxic.

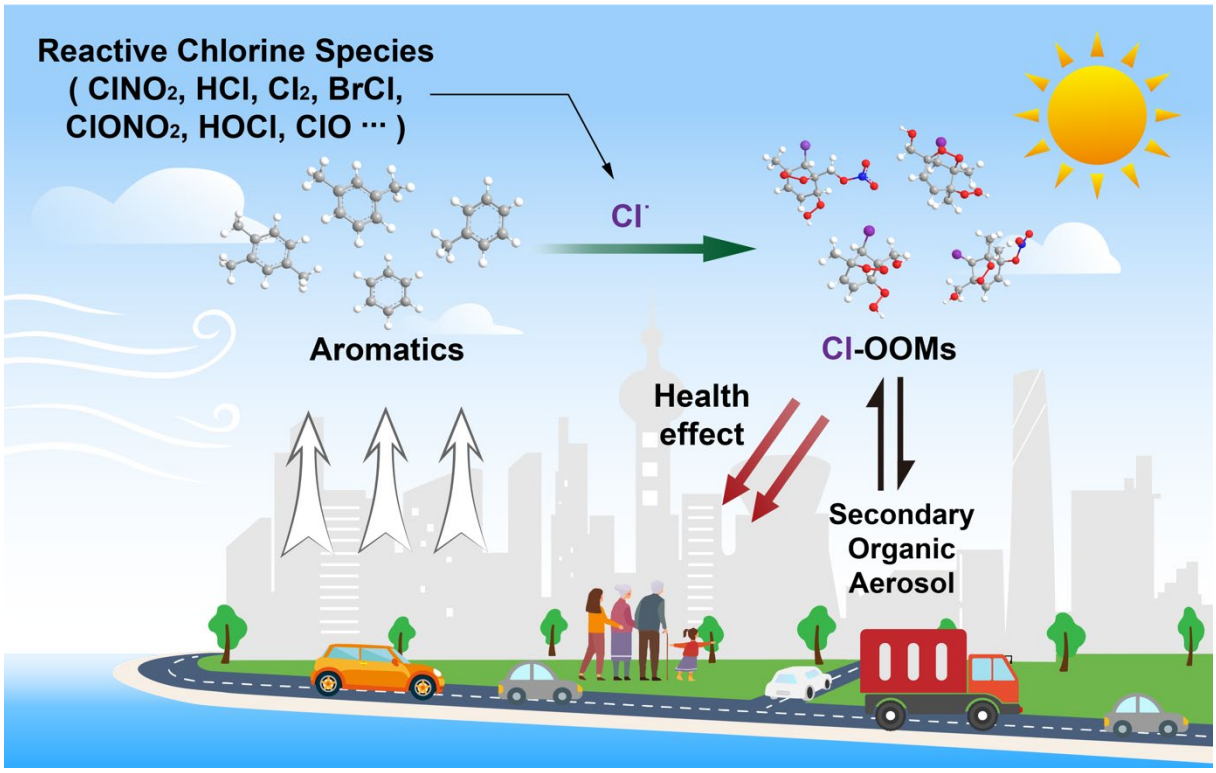

1. Introduction

Atmospheric chlorine atoms (Cl), together with hydroxyl radicals (OH), ozone (O_3), and nitrate radicals (NO_3), play vital roles in transforming volatile organic compounds (VOCs), leading to the formation of oxygenated organic molecules (OOMs) and secondary organic aerosol (SOA)(Priestley et al., 2018; Shang et al., 2021; Tham et al., 2016; Thornton et al., 2010). The involvement of Cl atoms in atmospheric chemical processes was conventionally thought to be confined to the oceanic boundary layer (Keene et al., 1999; Knipping et al., 2000). Estimated Cl atom concentrations in the coastal region ranged from 10^2 to 10^5 molecules cm^{-3} (Thornton et al., 2010; Wingenter et al., 2005). Recently, a number of reactive chlorine species, such as nitryl chloride ($ClNO_2$), chlorine nitrate ($ClONO_2$), hypochlorous (HOCl), chlorine (Cl_2), bromine chloride (BrCl), and hydrochloric acid (HCl), were found to lead to high concentrations of Cl atoms in the urban and suburban atmospheres (Breton et al., 2018; Peng et al., 2020; Priestley et al., 2018). During the daytime, peak Cl atom concentrations can reach 10^6 molecules cm^{-3} (Wang et al., 2023). which is still less than the global average concentrations of OH radicals (Breton et al., 2018; Liu et al., 2017). Nonetheless, the reaction rate coefficients of VOCs with Cl atoms are generally 1-2 orders of magnitude larger than those of OH radicals, which can partially compensate for the lower concentration of Cl atoms when determining the relative importance of different reactive loss pathways of VOCs (Chen et al., 2023; Riva et al., 2015; Wang et al., 2005).

Apart from H-abstraction, Cl atoms can be added to VOCs forming chlorine-containing oxygenated organic molecules (Cl-OOMs) in reactions of VOCs with Cl atoms. For small alkenes (e.g., isoprene), the reaction mechanism is dominated by Cl-addition to the double bond, with some allylic hydrogen abstraction (approximately 15% for isoprene at 1 atm) (Finlayson-Pitts et al., 1999; Orlando et al., 2003; Ragains and Finlayson-Pitts, 1997). For larger biogenic VOCs (e.g., β-pinene), which contain a greater number of abstractable hydrogen atoms, H-abstraction becomes more significant; for instance, H-abstraction is thought to account for half of the overall initiation reactions (Finlayson-Pitts et al., 1999). Overall, both Cl-addition and H-abstraction pathways coexist for biogenic VOCs, with the Cl-addition pathway possibly

being the more dominant pathway, such as isoprene (Wang et al., 2022) and d-limonene (Wang et al., 2019).

Given the ubiquitous existence of aromatics in the urban air and the recent detection of reactive chlorine species that are precursors of Cl atoms in the same atmosphere, the reaction mechanisms of aromatics and Cl atoms should be of concern. Although the reaction rate coefficient of benzene with Cl atoms under normal atmospheric conditions is relatively slow (1.3×10^{-15} cm^3 $molecule^{-1}$ s^{-1}) and this reaction is insignificant in the ambient atmosphere, its reaction mechanism provides valuable insights into reaction pathways of Cl atoms and aromatics (Shi and Bernhard, 1997). Sokolov *et al.* proposed that C_6H_6Cl radicals, formed through a Cl-addition pathway in reactions of Cl atoms and benzene, can either decompose back to benzene or further react in a non-aromatizing manner (Sokolov et al., 1998). In contrast, toluene, xylene, and trimethylbenzene react with Cl atoms at faster rates, urging a better understanding of their reaction mechanisms. Using the density functional theory and the conventional transition state theory, Huang *et al.* investigated the Cl-toluene reaction (Huang et al., 2012). Their findings indicate that the reaction rate coefficient for the H-abstraction pathway (5.58×10^{-11} cm^3 $molecule^{-1}$ s^{-1}) is substantially higher than that for the Cl- addition pathway (0.91×10^{-11} cm^3 $molecule^{-1}$ s^{-1}), highlighting the significance of the H-abstraction pathway that accounts for approximately 86% of Cl-initiated reactions. Studies employing gas chromatography-mass spectrometry (GC-MS) to examine products of Cl-initiated reactions of toluene and iodide-based chemical ionization mass spectrometry (I-CIMS) to analyze products of Cl-initiated reactions of m-xylene, have both predominantly detected chlorine-free oxygenated organic compounds, which were supposed as main products (Cai et al., 2008; Wang et al., 2005). These results have guided atmospheric models to integrate the H-abstraction as the primary reaction pathway in their analytical frameworks (Ma et al., 2023; Peng et al., 2022). However, studies focusing on the Cl-addition pathway and its related products are sparse, and the significance of the Cl-addition pathway in the atmospheric reactions of Cl atoms and aromatics remains elusive. Over the past decade, thanks to the development of nitrate-based chemical-ionization atmospheric-pressure-interface long-time-of-flight mass spectrometers

(nitrate-CI-APi-LToF), there have been significant advancements in the detection of highly oxygenated organic molecules and radicals, which is crucial for elucidating the mechanisms of Cl-initiated reactions with VOCs (Bianchi et al., 2019; Ehn et al., 2010). The formation of highly oxygenated organic products, including Cl-containing ones from the reactions of biogenic VOCs with Cl atoms, were gradually revealed, whereas whether or not significant amounts of Cl-containing highly oxygenated organics and radicals can be formed from Cl atoms and aromatics remains unclear (Wang et al., 2020).

OOMs can lead to potential air quality, climate, and health effects. Due to their low volatility, OOMs have been identified as dominant precursors for the growth of newly formed particles and formation of SOAs, which are known for their negative effect on air quality and climate impacts (Ehn et al., 2014; Kulmala et al., 2013). Compared to non-chlorine-containing OOMs (non-Cl-OOMs), Cl-OOMs formed through the introduction of chlorine substituents make organic compounds more lipophilic, facilitating their interactions with hydrophobic sites and promoting enzymatic biotransformation in general, which can lead to adverse health effect in turn (Henschler, 1994; Zhang et al., 2019). Therefore, field and laboratory studies for characteristics and sources of Cl-OOMs from the reactions of Cl-aromatics and their risk assessment upon human atmospheric exposure should be carried out.

In this study, we investigated non-Cl-OOMs and Cl-OOMs formation mechanisms from Cl-initiated reactions of toluene, m-xylene, and 1,2,4-trimethylbenzene (1,2,4-TMB) in the presence and absence of NO_x in a laboratory flow reactor, using a nitrate-CI-APi-LToF (Aerodyne Research, Inc. USA, and Tofwerk AG, Switzerland) and a Vocus proton-transfer-reaction long-time-of-flight mass spectrometer (Vocus-PTR-LToF) (Tofwerk AG, Switzerland). In addition, the nitrate CI-APi-LToF was also deployed in a field campaign in suburban Shanghai during winter to search for ambient gaseous Cl-OOMs. The toxicity of selected Cl-OOMs, which were simultaneously detected both in laboratory experiments and ambient observations, was evaluated by computational toxicity.

2. Materials and methods

2.1. Experimental Set-up in the Laboratory.

A general scheme of the experimental setup is shown in Figure S1. Simulation experiments were conducted in a 6 L quartz flow tube reactor with a total flow rate of 10 L min^{-1}, resulting in a residence time of ~36 seconds. This flow tube is covered by aluminum composite panels to avoid room light. Zero air with relative humidity (RH) less than 1% generated from a Zero Air Generator (AADCO Instruments, Inc. USA) was used as carrier gas. The reaction temperature was maintained at around 20°C.

Homemade aromatics–N_2 cylinders were prepared from their liquid standards (toluene, ≥ 99.0%, Aladdin; m-xylene, ≥ 99.0%, Aladdin; 1,2,4-TMB, ≥ 99.5%, Aladdin) together with high-purity nitrogen gases. Cl atoms were produced by photolysis of chlorine (Cl_2, Shanghai Wetry Standard Reference Gas Analytical Technology Co., LTD) using 350 nm UV lights. In experiments with NO_x, NO (Air Liquid Co., LTD) was added into the flow tube to produce and sustain NO_x mixing ratios that were sufficiently high to be a competitive sink for RO_2 radicals. RH is controlled by changing zero air flowrates through the water bubbler. Before each experiment, the wall of the flow tube was cleaned with a water/alcohol solution and then purged with zero air for over 1 hour. Details of the experimental setup are provided in Text S1 of the Supporting Information.

The concentration of Cl atoms was controlled by adjusting the flow rate of Cl_2. The mean concentrations of Cl atoms were determined according to the decay of aromatic precursors (Figure S2) and calculated using Eq.(1), with reaction rate coefficients k of 6.2×10^{-11} cm^3 $molecule^{-1}$ s^{-1}, 1.35×10^{-10} cm^3 $molecule^{-1}$ s^{-1}, and 2.42×10^{-10} cm^3 $molecule^{-1}$ s^{-1} for reactions between Cl atoms and toluene, m-xylene, and 1,2,4-TMB, respectively(Wang et al., 2005), as follows:

$$[Cl] = -1/kt \times \ln([Aromatics]_t/[Aromatics]_0) \quad \text{Eq. (1)}$$

where $[Aromatics]_0$ and $[Aromatics]_t$ are the initial concentration and the concentration after a reaction time t of aromatic precursors, respectively. $[Cl]$ is the estimated concentration of Cl atoms in the flow tube. In our flow tube experiments, the extent of oxidation is quantified using the parameter of Cl exposure, defined as $[Cl]$ multiplied by the reaction time t. Cl exposures in our experiments were in the range of (1.2-2.0) $\times10^9$ molecules cm^{-3} s, equivalent

149 to atmospheric oxidation times of roughly 0.6-1.3 hours for aromatics at a daytime Cl atom
150 concentration of 5×10^5 molecules cm^{-3} (Chang et al., 2004; Tham et al., 2016; Wang et al.,
151 2023).

152 A Vocus-PTR-LToF and a nitrate-CI-APi-LToF (more details refer to Text S2 & Figure S3
153 in Supporting Information) were simultaneously deployed to detect aromatic precursors and
154 gaseous OOM products, respectively. In addition, an iodide-CIMS (I-CIMS, Tofwerk AG,
155 Switzerland) was used in a separate experiment focusing on the m-xylene + Cl system to expand
156 the detection of Cl-initiated reaction products. Their working principles were described in
157 details elsewhere (Eisele and Tanner, 1993; Krechmer et al., 2018). Signals of aromatic
158 precursors and reaction products measured from the zero air were treated as their background.
159 The resolving power of the nitrate CI-APi-LToF was up to around 8000 for ions with m/z larger
160 than 200 Th. The ions of NO_3^-, $HNO_3 \cdot NO_3^-$, and $C_6H_5NO_3 \cdot NO_3^-$ were selected for mass
161 calibration, and the calibration error is less than 1ppm. When identifying the OOM signal peaks,
162 the error is limited below 4 ppm.

163 OOM concentrations are estimated by Eq. (2)(Kürten et al., 2016),

$$[OOMs] = C \times \frac{OOM \cdot {NO_3}^-}{{NO_3}^- + HNO_3 \cdot {NO_3}^- + (HNO_3)_2 \cdot {NO_3}^-} \times T \qquad \text{Eq. (2)}$$

164

165 where $OOM \cdot NO_3^-$, NO_3^-, $HNO_3 \cdot NO_3^-$, and $(HNO_3)_2 \cdot NO_3^-$ represent signals of corresponding
166 ions in units of counts per second (cps). OOMs with an oxygen content of equal to or more than
167 6 (i.e., highly oxygenated organic molecules, HOMs) are assumed to cluster with NO_3^- at the
168 same rate coefficient as that of sulfuric acid (H_2SO_4), i.e., both at collision-limited rates
169 (Bianchi et al., 2019; Ehn et al., 2010). Therefore, the calibration factor *C* for sulfuric acid is
170 adopted as that of OOMs (Kürten et al., 2011, 2012). It should be noted we also used the same
171 calibration factor C for quantification of OOMs with an oxygen number of less than 6, which
172 may lead to relatively high uncertainties (Alage et al., 2024). A mass-dependent transmission
173 correction factor *T* of our instrument is also taken into account in this study (Heinritzi et al.,
174 2016). The mass-dependent transmission correction factor is instrument-specific and
175 determined by depleting the primary ion with a series of perfluorinated acids and comparing

the primary ion signal depletion with the product signal increase (which would match for equivalent transmission efficiency) (Lu et al., 2020).

In addition, a NO_x monitor (Thermo, 49i) was utilized to measure NO_x concentrations in laboratory experiments. A nano-SMPS (Scanning Mobility Particle Sizer with a nano Differential Mobility Analyzer, TSI, USA) together with a PSM (Particle Size Magnifier, Airmodus, Finland) were used to detect particles in the range of sub-3 nm to 60 nm, indicating the absence of newly formed particles during all experiments.

Table 1 summarizes experimental conditions including mixing ratios of aromatic precursors (i.e., toluene, m-xylene, and 1,2,4-TMB), NO_x, and RH.

Table 1. Summary of experimental conditions in the laboratory experiments.

Exp.	Precursor	Initial precursor concentration (ppb)	Initial NO [a] (ppb)	Estimated Cl exposure ($\times 10^9$ molecule cm^{-3} s)	RH [b] (%)	Non-Cl-OOMs molar yield (%)	Cl-OOMs molar yield (%)	Ratio (Cl-OOMs/ Total OOMs, %)	Ratio (Dimer/ Monomer, %) [c]
1	Toluene	80	0	2.0	<1	5.1	2.4	32	3.5
2	Toluene	80	0	1.2	60	0.7	0.3	31	2.0
3	Toluene	84	45	2.7	<1	6.8	2.6	28	1.7
4	Toluene	80	40	1.6	60	1.8	0.8	29	1.0
5	m-Xylene	87	0	2.0	<1	0.6	0.5	43	3.2
6	m-Xylene	87	0	1.6	68	0.3	0.2	44	2.6
7	m-Xylene	90	45	1.7	<1	1.4	0.6	31	0.9
8	m-Xylene	87	50	2.3	35	1.1	0.5	32	1.2
9	1, 2, 4-TMB	98	0	1.4	<1	0.5	0.3	34	2.1
10	1, 2, 4-TMB	103	0	1.4	30	0.3	0.2	35	1.4
11	1, 2, 4-TMB	93	40	2.2	<1	1.5	0.7	31	0.8
12	1, 2, 4-TMB	109	55	2.2	30	1.0	0.6	37	0.6

[a] In the presence of NO experiments, there is more OH chemistry was involved in Cl-aromatics reactions and its influence can lead to relatively high uncertainty in the molar yields reported in the table for pathways influenced by OH chemistry. Approximately 90% of NO was converted into NO_2 after the UV light was turned on.

[b] Relative humidity.

[c] The molar yield ratios of total OOM dimers to monomers. Monomers are defined as molecules with a carbon number equal to the carbon number of aromatic precursor (nC), and dimers are defined as molecules with carbon numbers ranging from 2nC -1 to 2nC +1.

2.2. Field measurements.

A field campaign was conducted from December 14th, 2022, to February 2nd, 2023, at the Dianshan Lake (DSL) Air Quality Monitoring Supersite in suburban Shanghai, China (31.10°N,120.98°E). This monitoring site is frequently impacted by regional transport and experiences episodes of anthropogenic pollution. A detailed description of this site can be found elsewhere (Wu et al., 2023; Yang et al., 2022, 2023). A Vocus-PTR-LToF and a nitrate-CI-APi-LToF were both deployed in this field campaign to detect aromatics and Cl-OOMs, respectively. The detailed description of nitrate-CI-APi-LToF and Vocus-PTR-LToF, and their calibration in the field measurement are shown in the Supporting Information (Text S2).

2.3. Heath effect estimation.

A number of Cl-OOMs were assessed using the Estimation Program Interface Suite (EPI, V. 4.11) and Toxicity Estimation Software Tool (T.E.S.T, V. 5.1.2) software provided by the United States Environmental Protection Agency (EPA), to estimate their persistence, bioaccumulation, and toxicity through calculated half-life for reactions with OH, bioconcentration factors (BCF), oral rat pLD_{50} (-log10(pred), mol/kg), developmental toxicity, and mutagenicity. The models utilized the SMILES (Simplified Molecular Input Line Entry System) notation of the target compounds as input for the prediction.

3. RESULTS AND DISCUSSION

3.1. OOM molar yields.

The molar yields of OOMs are determined as OOMs formed (ΔM, molar cm^{-3}) divided by precursor reacted (ΔAr, molar cm^{-3}):

$$Molar\ yield = \frac{\Delta M}{\Delta Ar} \qquad \text{Eq. (3)}$$

Table 1 summarizes non-Cl-OOMs' and Cl-OOMs' molar yields and OOMs' dimer-to-monomer ratios from our laboratory experiments. The molar yields of non-Cl-OOMs and Cl-OOMs from reactions of three aromatic precursors with Cl atoms in the absence of NO_x are within the ranges of 0.3-5.1% and 0.2-2.4%, respectively. These values are comparable with previously reported: HOM molar yields (0.8-4.0%) detected by nitrate-CI-APi-LToF for the reactions between α-

pinene and Cl atoms (Wang et al., 2020) and non-Cl-OOMs molar yields (4.4-8.8%) detected by H_3O^+-Chemical Ionization Mass Spectrometry (H_3O^+-CIMS) for the reactions between m-xylene and Cl atoms (Bhattacharyya et al., 2023). The low molar yields observed in both this study and previous studies may be attributed to the preference of different detection techniques. Nevertheless, the observed ratio of Cl-OOMs to non-Cl-OOMs, ranging from 29% to 44% (Table 1), further indicates the non-negligibility of the Cl-OOMs products among the total OOMs products. In the presence of 40-55 ppb NO_x, our flow tube experiments show that the molar yields of non-Cl-OOMs and Cl-OOMs from three aromatics are within the ranges of 1.0-6.8% and 0.5-2.6%, respectively. The addition of NO_x can slightly increase the molar yields of both non-Cl-OOMs and Cl-OOMs.

Typically, the fate of peroxy radicals in flow tube experiments is largely influenced by their reactions with other RO_2, HO_2, or NO species, which are contingent upon the specific experimental conditions (Bianchi et al., 2019; DeMore et al., 1997). In experiments without NO_x, while the termination of RO_2 was primarily anticipated to be governed by RO_2-RO_2 and HO_2-RO_2 reactions. However, after the addition of NO_x, the reaction between RO_2 and NO tended to predominate, leading to a reduction in the dimer-to-monomer ratio by 50.5% (Exp. 3 and Exp. 1 in Table 1).

In contrast to OH reaction, the presence of Cl, ClO, and Cl_2 in chlorine-involved reaction may introduce additional reaction pathways related to Cl-OOM formation. However, these pathways make only minor contributions to the formation of Cl-OOMs under our experimental conditions (see Text S4 in Supporting Information for detailed analysis).

Although both the non-Cl-OOMs and Cl-OOMs molar yields increased in the presence of NO_x, the ratio of Cl-OOMs to the total OOMs decreased when NO_x was added. This phenomenon can be attributed to the significant contribution of OH chemistry, primarily resulting from the NO + HO_2 reaction. The additional OH radicals can contribute to the formation of non-Cl-OOMs, as supported by recent experimental and modeling studies on the reaction dynamics between Cl atoms and isoprene (Wang et al., 2022). For our experiments, as NO_x was added into the flow tube, the concurrent presence of Cl atoms, OH radicals, and

aromatics led to a notable increase in the total OOM molar yields, ranging from 25 to 187%, while reducing the ratios of Cl-OOMs to the total OOMs by approximately 9-28% (Table 1). In addition, the increased Cl-OOM yields under NO_x conditions may result from the suppression of dimer or multimer formation (Table 1), which shifts the product distribution toward monomeric Cl-OOMs and thus leads to potential higher apparent yields. Moreover, NO_x-promoted chemistry facilitates the formation of nitrogen-containing OOMs with diverse structures and functionalities. The nitrate-CI-APi-LToF exhibits different detection sensitivities toward these species, which may also influence the estimated molar yields under high NO_x conditions. Besides, high RH leads to low molar yields, which may be attributed to the depressed detection efficiency of OOMs and the elevated vapor wall loss under humid conditions (Huang et al., 2018). The product distribution remains unchanged under high humidity conditions (see Figure 1B and Figure S4), indicating that the presence of water does not significantly influence the reaction between Cl atoms and aromatics.

3.2. Characteristics of OOM products and peroxyl radicals.

Mass defect plots of stabilized products from reactions between toluene (Exp.1 in Table1), m-xylene (Exp.5 in Table1), and 1,2,4-TMB (Exp.9 in Table1) and Cl atoms in the absence of NO_x are shown in Figure 1. These products display similar distribution patterns, consisting of monomers (with carbon numbers equal to carbon numbers of the precursor, nC) and dimer products (with carbon numbers ranging from 2nC -1 to 2nC +1). The ratio of dimer products to monomer products are 3.5%, 3.2%, and 2.1% for reactions of toluene, m-xylene, and 1,2,4-TMB with Cl atoms, respectively. Meanwhile, the products also can be classified into two groups: non-Cl-OOMs in blue and Cl-OOMs in orange in Figure 1. In general, the total concentration of Cl-OOMs is lower than that of non-Cl-OOMs. Specifically, the concentrations of Cl-OOMs account for 47%, 91%, and 52% of the non-Cl-OOMs in the toluene, p-xylene, and 1,2,4-trimethylbenzene experiments, respectively. Both non-Cl-OOMs and Cl-OOMs products can be categorized into several bands, as indicated by the dashed lines in Figure 1, each of which comprises compounds with varying numbers of oxygen atoms.

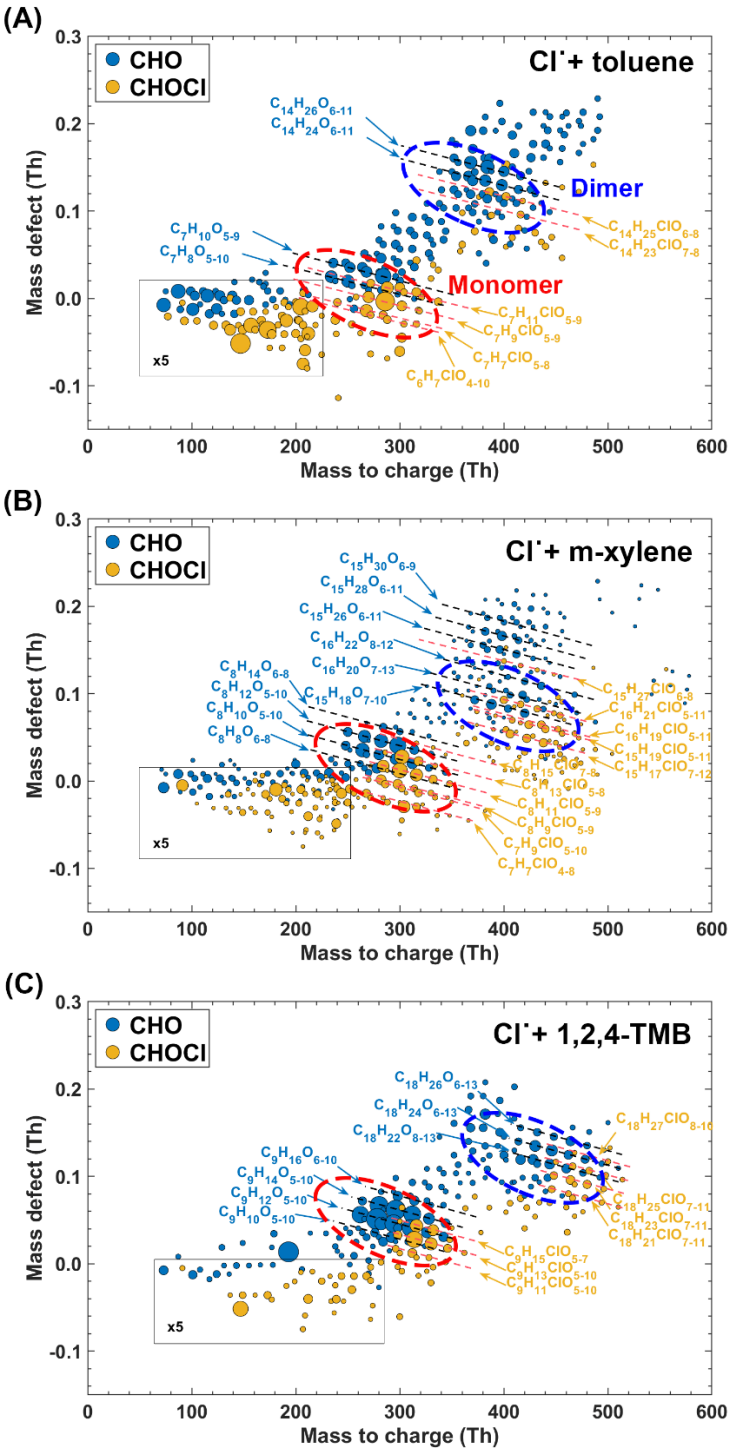

Figure 1. Mass defect plots of OOM products detected by a nitrate-CI-APi-LTOF from Cl-initiated reactions of (A) toluene, (B) m-xylene, and (C) 1,2,4-trimethylbenzene, respectively, in the absence of NO_x. The detected products are marked by their exact mass (with NO_3^- reagent ions) and mass defect (exact mass subtracted by its unit mass). The lines annotate the general chemical formulae. Chlorine-containing and non-chlorine-containing formulae are shown in different colors. The size of the circle corresponds to the concentration of products.

The mass spectrum of the detected OOMs monomer and dimer products from the reaction between m-xylene and Cl atoms with and without NO_x (Exp. 5&7 in Table 1) are shown in Figure 2. Without NO_x, dominant monomer products for non-Cl-OOMs included $C_8H_{10}O_6$ and $C_8H_{12}O_{6\text{-}8}$, whereas for Cl-OOMs, $C_8H_{11}ClO_{6\text{-}8}$ and $C_8H_{13}ClO_{6\text{-}7}$ dominated. The most abundant dimer compounds for non-Cl-OOMs were $C_{16}H_{20}O_9$, $C_{16}H_{22}O_{10}$, and $C_{15}H_{18}O_8$, whereas for Cl-OOMs, $C_{16}H_{19}ClO_{8,10}$, $C_{16}H_{21}ClO_9$, and $C_{15}H_{17}ClO_8$ prevailed. Dimer products containing two Cl atoms were also observed, exemplified by $C_{16}H_{18,20}Cl_2O_{10}$. Under NO_x-present conditions, the main non-Cl-OOMs included $C_8H_{11}NO_{6\text{-}10}$ and $C_8H_{12}N_2O_{10}$, whereas Cl-OOMs were represented by $C_8H_{10}ClNO_{7\text{-}8}$ and $C_8H_{11}ClN_2O_{9\text{-}10}$.

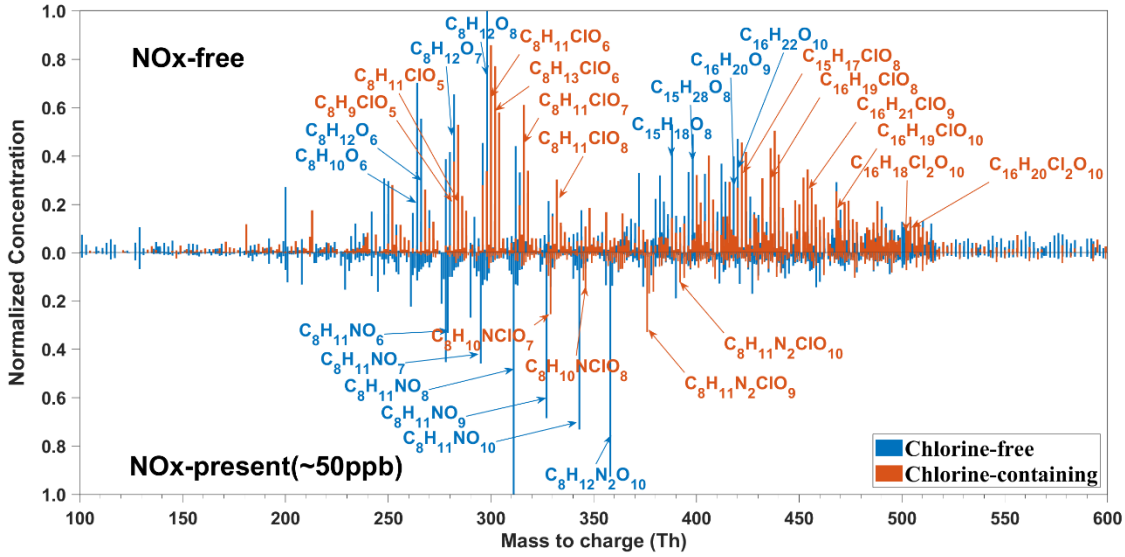

Figure 2. Mass spectra of OOM products detected by a nitrate-CI-APi-LToF from the reaction of m-xylene and Cl atoms under NO_x-free and NO_x-present conditions. The y-axes in both figures are standardized by setting their maximum concentrations to 1.

Moreover, 29 peroxyl radicals in total were observed in our flow tube experiments with three precursors, as listed in Table S1 and illustrated in Figures 3 & S5. It is crucial to note, however, that not every intermediate radical formed could be conclusively identified. This is primarily due to the inherent instability and the extremely brief life span of peroxyl radicals, which pose significant challenges for their detection. Currently, the absolute concentrations of radicals measured by I-CIMS cannot be reliably quantified. Therefore, for visualization and

comparative purposes, the signal intensities of the radicals $C_8H_{10}ClO_{2-3}$ detected by I-CIMS were normalized to match the signal intensity of $C_8H_{10}ClO_4$ measured by nitrate-CI-APi-LToF, as presented in Figure 3. It is essential to note that this normalization was solely used to facilitate consistent visual comparison across instruments. Consequently, the normalized I-CIMS signals are not utilized for quantitative comparisons of radical concentrations in the subsequent discussion.

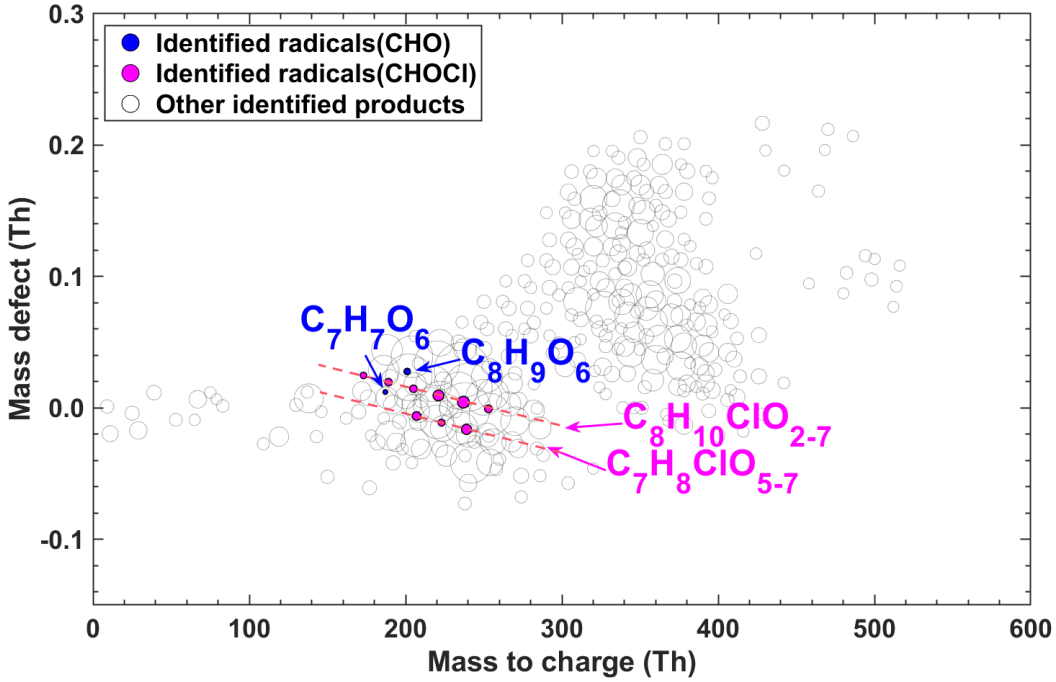

Figure 3. Mass defect plot of peroxyl radicals detected by a nitrate-CI-APi-LToF and an I-CIMS from Cl-initiated reactions of m-xylene without NO_x. $C_8H_{10}ClO_{2-3}$ were detected by I-CIMS while the remaining radicals were observed using nitrate-CI-APi-LToF. The detected products are marked by their exact mass (with NO_3^- reagent ions) and mass defect (exact mass subtracted by its unit mass). The lines annotate the general chemical formulas. Chlorine-containing and non-chlorine-containing formulas are shown in different colors. The size of the circle is proportional to the concentrations of peroxyl radicals.

Take the reaction between Cl atoms and m-xylene in the absence of NO_x for example, we detected peroxyl radicals including $C_8H_{10}ClO_{2-7}$, $C_7H_8ClO_{5-7}$, $C_8H_9O_6$, and $C_7H_7O_6$ (Figure 3 & Figure S5). High-resolution peak fittings of partial peroxy radicals from the raw mass spectrum obtained by nitrate-CI-APi-LToF are shown in Figure S6. Notably, the dominant species among these radicals was $C_8H_{10}ClO_6$, constituting 27.4% of the total signal of identified peroxyl radicals in the reaction of Cl atoms and m-xylene and nearly three times of the $C_8H_9O_6$

radical signal. Also, similar ratio rules of chlorine-containing radicals (analogy of $C_8H_{10}ClO_6$) to non-chlorine-containing radicals (analogy of $C_8H_9O_6$) were observed for toluene (~4.2 times) and 1,2,4-TMB (~3.8 times). Although $C_7H_8ClO_{5\text{-}7}$ radicals were also discernible, their signal intensity was merely 22.3% of the total signal of identified peroxyl radicals in the reaction of Cl atoms and m-xylene. Non-Cl-containing radicals were also detected, albeit with substantially lower signal values, accounting for only 15.5% of the total identified radical signals.

3.3. Formation mechanisms of Cl-OOMs

3.3.1. Cl-addition pathway

Given the similar product patterns for the three precursors (toluene, m-xylene, and 1,2,4-TMB), it is reasonable to infer that the reaction mechanisms between different aromatics and Cl atoms are analogous. A generalized mechanism is thus proposed, elucidating the Cl-initiated reactions of m-xylene in the absence of NOx, as depicted in Scheme 1. This scheme serves as a representative example highlighting the potential pathways involved in the Cl-initiated reactions of aromatics.

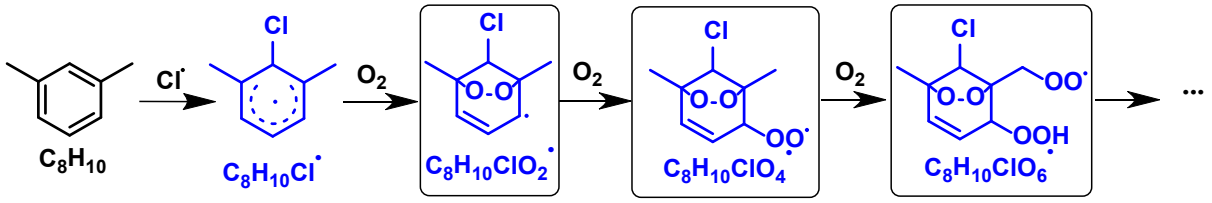

Scheme 1. Proposed reaction mechanisms of m-xylene with Cl atoms leading to the formation of Cl-OOMs. Radicals detected by nitrate-CI-APi-LToF are marked with black boxes.

Although the theoretical studies by Huang *et al.* (2012) show that the Cl-addition pathway accounts for only 14% of Cl-initiated reactions of toluene (298K), which is significantly lower than the 86% attributed to the H-abstraction pathway, the proportion of Cl-OOMs products from Cl-addition reaction should not be overlooked, as evidenced by the observation of peroxyl radicals and product distribution characteristics in this study (Huang et al., 2012). The initial reaction of m-xylene (C_8H_{10}) with Cl atoms can occur through two pathways: the Cl-addition pathway, leading to the formation of a $C_8H_{10}Cl$ radical ($C_8H_{10}Cl\cdot$, refer to Scheme 1) or the H-

abstraction pathway, forming a C_8H_9 radical (C_8H_9·, refer to Scheme S1) and C_8H_9 radical ($C_8H_9O_2$·refer to Scheme S1). Then, both C_8H_9· and $C_8H_{10}Cl$· can in turn undergo autoxidation via the H-shift and addition of O_2 to produce peroxy radicals of $C_8H_{10}O_5$· or $C_8H_{10}ClO_6$·(Vereecken and Nozière, 2020; Bianchi et al., 2019). The peroxyl radical $C_8H_{10}ClO_6$· was identified as the predominant species in terms of signal (Table S1). Although these Cl-OOMs-to-non-Cl-OOMs signal ratios may not accurately represent their relative concentrations due to sensitivity differences of these radicals towards the reagent ions ($(HNO_3)_{0\text{-}1}\cdot NO_3^-$), it is still noteworthy that these Cl-RO_2 overlooked in previous studies were directly observed in such a reaction system, thereby suggesting that Cl-addition pathway is indeed present in the initial reaction steps of reactions between Cl atoms and aromatics.

In the reaction of Cl atoms and m-xylene, a certain fraction of the peroxyl radicals ($C_8H_{10}ClO_6$·) might also be derived from the secondary Cl-addition reaction between Cl atoms and a first-generation stabilized product $C_8H_{10}O_6$ (Scheme 1). Indeed, it is challenging to evaluate the exact contribution from secondary Cl-addition reaction to the formation of $C_8H_{10}ClO_6$·. However, it may be indirectly assessed via the potential secondary reactions between more dominant first-generation stabilized products ($C_8H_{12}O_x$) and Cl (Table S2), since $C_8H_{10}O_6$ and $C_8H_{12}O_x$ likely react with Cl at similar rates. If secondary Cl-addition reactions were significant in the reaction system of Cl atoms and m-xylene, $C_8H_{12}O_x$ should undergo secondary Cl-addition reactions to generate $C_8H_{12}ClO_x$ radicals. Yet, $C_8H_{12}ClO_x$ radicals were not detectable, which hints that secondary Cl-addition reactions could only play a minor role in our experiments. Therefore, it appears that the secondary Cl-addition reactions between stabilized products and Cl atoms are less significant compared with Cl-addition in the initial reaction steps.

Recently, Jahn et al. (2024) investigated the formation of secondary organic aerosols from the reaction of ethylbenzene and Cl atoms, and attributed the observed Cl-addition products to reactions involving non-aromatic C=C bonds (Jahn et al., 2024). They claimed that OH radical existed in their experiments, due to the presence of NOx. As a result, approximately 40% of ethylbenzene reacted with Cl atoms, 30% with OH, and 30% remained unreacted. Thus, a

secondary Cl addition to $C_8H_{11}NO_6$ for reaction of ethylbenzene and Cl atoms, forming $C_8H_{12}ClNO_8$, is possible (Scheme S1). In our experiments, although OH radicals can still be generated through H-abstraction from methyl groups by HO_2 (Bhattacharyya et al., 2023), the use of 20 ppm CO as an OH scavenger confirmed the presence of OH chemistry in our system. Nevertheless, the stable real-time signals of first-generation products and radicals from the Cl-addition reaction, observed both with and without OH chemistry, provide compelling evidence that the Cl-addition pathway remains the dominant mechanism for Cl-RO_2 formation under low-NO_x conditions (see Text S5 in the Supporting Information). Moreover, under high NO_x conditions in our experiments, the dominant Cl-OOMs $C_8H_{10}ClNO_7$ (Scheme S2), contains two fewer H atoms than the $C_8H_{12}ClNO_8$ proposed by Jahn et al. (2024) as a secondary Cl-addition product (Scheme S3). While this difference might suggest the presence of an additional double bond or a ring in $C_8H_{10}ClNO_7$, it could also result from multi-generation oxidation chemistry. Specifically, H-abstraction from a carbon bearing an OH or OOH can form a carbonyl, thereby reducing the hydrogen count without requiring a new double bond.

3.3.2. Autoxidation and subsequent reactions of Cl-RO_2

Scheme 2 shows a proposed reaction mechanism for the autoxidation of the main Cl-RO_2 radical ($C_8H_{10}ClO_4\cdot$) generated from Cl atoms and m-xylene. Autooxidation of $C_8H_{10}ClO_4\cdot$ leads to $C_8H_{10}ClO_6\cdot$. There are two distinct isomeric forms of $C_8H_{10}ClO_6\cdot$, denoted as $C_8H_{10}ClO_6\cdot$(I) and $C_8H_{10}ClO_6\cdot$(II), which is similar to results for aromatics + OH by Molteni et al (Molteni et al., 2018). Notably, the formation of $C_8H_{10}ClO_6\cdot$(II) requires a second step of endo-cyclization, which is not competitive on account of its slow reaction rate, as inferred from several previous studies using both experimental and theoretical approaches of OH-initiated oxidation of aromatics (Wang et al., 2017; Xu et al., 2020). Therefore, the abundance of $C_8H_{10}ClO_6\cdot$(I) would likely be much higher than $C_8H_{10}ClO_6\cdot$(II), and our following discussion primarily focuses on the subsequent reaction processes involving $C_8H_{10}ClO_6\cdot$(I). Briefly, $C_8H_{10}ClO_6\cdot$ reacts with $RO_2\cdot$ to generate $C_8H_{9,11}ClO_5$ and $C_8H_{10}ClO_5\cdot$ (Reaction pathway *R2b*) and with an HO_2 radical to produce $C_8H_{11}ClO_6$ (Reaction pathway *R2c*). Meanwhile, $C_8H_{10}ClO_6\cdot$ has no more H atoms for another H-shift at an appreciable rate based on our current

understanding.(Wang et al., 2024) In the presence of NO_x, $C_8H_{10}ClO_6\cdot$ is terminated (Reaction pathway *R2a*), leading to the formation of $C_8H_{10}ClNO_7$ products.

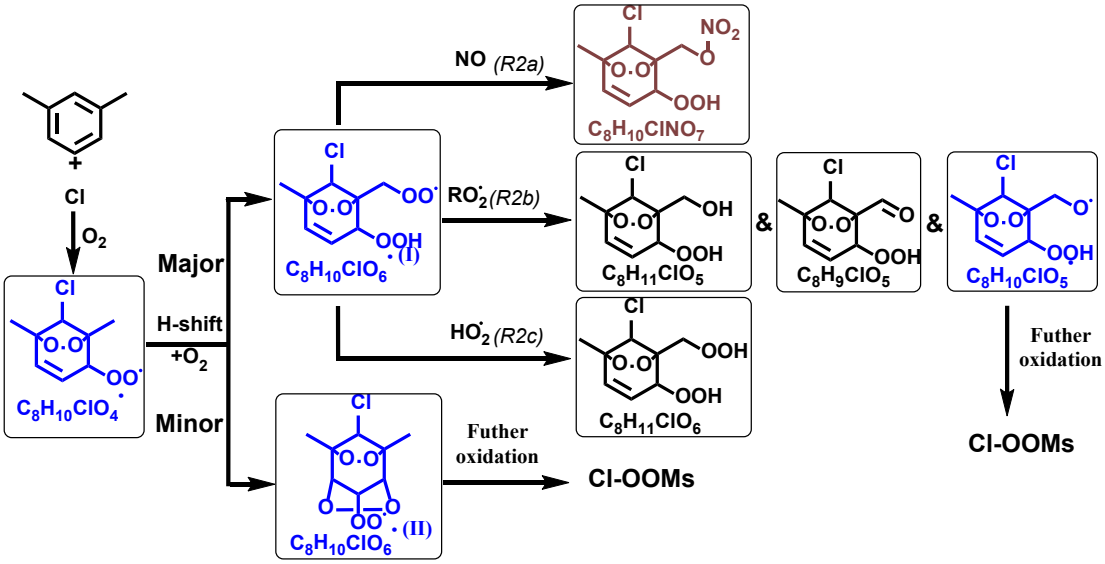

Scheme 2. Reaction pathways of the bicyclic peroxyl radical $C_8H_{10}ClO_4$ in the Cl-initiated reaction of m-xylene. Blue, brown, and black formulae denote radicals, nitrogen-containing products, and Cl-OOMs products, respectively. Radicals and stable products detected by nitrate-CI-APi-LToF are marked with black boxes.

3.3.3. Dimer formation

The accretion reaction ($RO_2 + R'O_2 \rightarrow ROOR' + O_2$) represents a pivotal source for dimer compounds, originating from highly oxidized and functionalized RO_2 radicals (Ehn et al., 2014; Zhao et al., 2018). As shown in Figure 2, $C_{16}H_{19}ClO_8$ and $C_{16}H_{19}ClO_{10}$ are two typical accretion reaction products from reactions between Cl atoms and m-xylene without NO_x. In detail, $C_{16}H_{19}ClO_{10}$ can be formed through the accretion reaction between $C_8H_{10}ClO_6\cdot$ and $C_8H_9O_6\cdot$ (Scheme 3). The formation pathways for $C_{16}H_{19}ClO_8$ are more varied compared to that of $C_{16}H_{19}ClO_{10}$. It can be produced either via the accretion of a $C_8H_{10}ClO_6$ radical with a $C_8H_9O_4$ radical or through the reaction of a $C_8H_{10}ClO_4$ radical with a $C_8H_9O_6$ radical. Meanwhile, $C_{16}H_{20}Cl_2O_{10}$, which is also detected during the reaction, can be formed via the accretion reaction of two $C_8H_{10}ClO_6$ radicals.

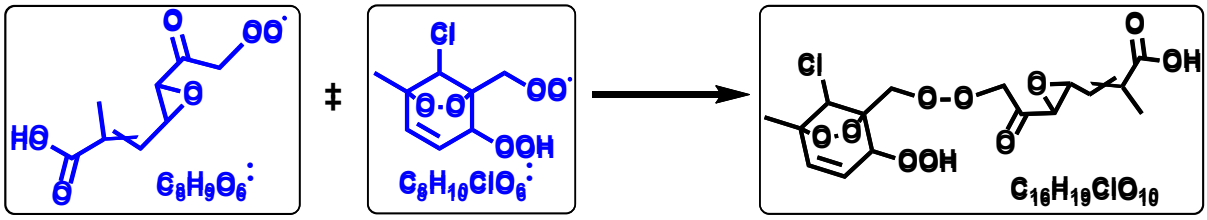

Scheme 3. Accretion reaction pathways of peroxyl radical $C_8H_{10}ClO_6\cdot$ and $C_8H_9O_6\cdot$ in the Cl-initiated reaction of m-xylene. Blue and black formulae denote radicals and stable products, respectively. Radicals and stable products detected by nitrate-CI-APi-LToF are marked with black boxes.

Previous studies have reported dimer formation rates during the OH-initiated oxidation of 1,3,5-trimethylbenzene, ranging from 1.4×10^{-10} to 25×10^{-10} cm^3 $molecule^{-1}$ s^{-1} (Berndt et al., 2017). Compared to the OH reaction, Cl-RO_2 is produced in the Cl atom reaction, but its reaction rate in the accretion reaction remains unknown. If Cl-RO_2 have lower reactivity (i.e., slower rate coefficients) for accretion reactions compared to non-Cl-containing RO_2, the same generation rate of Cl-RO_2 and RO_2 would result in higher concentration of Cl-RO_2, resulting in the high Cl-RO_2 signal detected. However, the generation rate of both Cl-RO_2 and RO_2 are currently uncertain, further complicating the determination of the chemical mechanisms of Cl-initiated reactions even more challenging.

3.4. Cl-OOMs detection in suburban Shanghai.

As shown in Figure 4A and Table S3, a total of 51 gaseous Cl-OOMs were identified during winter in suburban Shanghai, whose high-resolution peak fittings measured by nitrate CI-APi-LToF are shown in Figure S7. Figure S8 further demonstrates the accuracy of our peak identification by showing the ratio of the fitted peak intensities versus the peak separation for identified Cl-OOM peaks and adjacent ions from our ambient nitrate-CI-APi-LToF measurements (Cubison and Jimenez, 2015). The peak separation, normalized to the half-width at half-maximum ($\chi = \Delta t/HWHM$), is greater than 1 for all Cl-OOMs. Notably, 22% of the peaks exhibit χ values between 1 and 2, indicating they are separable but closely spaced, while 78% of the Cl-OOMs ($\chi > 2$) are well-separated peaks.

Ambient Cl-OOMs consist of compounds mostly with a single Cl atom and only two with two Cl atoms. The carbon and oxygen numbers of these Cl-OOMs ranged from 2 to 14 and 1

to 11, respectively. Figure 4B shows the abundance distribution of gaseous Cl-OOMs on the basis of carbon and oxygen numbers in their molecular formulae. Approximately 80% concentration of the identified Cl-containing molecules is C5-C9 Cl-OOMs, among which C6-C9 Cl-OOMs represent a large fraction of ~79 %. All assignments followed strict criteria for mass accuracy (< 4 ppm) and isotopic pattern matching. Interference screening with adjacent formulas (Table S4) was performed to ensure unambiguous identification. Nonetheless, the detection of these low-oxygenated Cl-OOMs should be interpreted with caution, and we acknowledge that their measured concentrations may carry higher uncertainty compared to those of more oxygenated compounds.

38 Cl-OOMs observed in field measurements were also identified in our laboratory experiments, corresponding to reaction products of Cl atoms with toluene, m-xylene, or 1,2,4-TMB. These results indicate that ambient C6-C9 Cl-OOMs exemplified by $C_7H_7N_2ClO_9$, $C_8H_{10}NClO_7$, and $C_9H_{15}ClO_8$ are likely formed from Cl-initiated reactions with aromatic compounds. On the other hand, isoprene was considered as a precursor of C5 Cl-OOMs (Breton et al., 2018; Priestley et al., 2018; Wang and Ruiz, 2017). Several relatively abundant ambient Cl-OOMs, specifically $C_2H_2Cl_2O_2$, $C_6H_4ClNO_{3\text{-}4}$, $C_8H_7ClO_6$, and C_9H_6ClNO (Figure 4A), although they were not observed in our flow tube experiments. The presence of $C_2H_2Cl_2O_2$ suggests possible contributions from the oxidation or atmospheric degradation of chlorinated solvents, combustion emissions, or industrial processes (Wang et al., 2021). The $C_6H_4ClNO_{3\text{-}4}$ may originate from Cl-induced reaction of aromatics. Similarly, $C_8H_7ClO_6$ and C_9H_6ClNO could be derived from more oxidized aromatic compounds undergoing multi-step oxidation or fragmentation. The observation of these species highlights the complexity and diversity of Cl chemistry in suburban environments, underscoring the importance of further studies integrating broader precursor sets, longer aging times, and additional reaction pathways to better understand their sources and formation mechanisms.

The diurnal profiles of all 51 Cl-OOMs identified in the ambient were shown in Figure S9. Similar to previous reports in northern Europe and Beijing (Breton et al., 2018; Priestley et al., 2018), Cl-OOMs increased with elevated solar radiation and their peaks appeared at around

12:00 p.m. (local time). This suggests that while $ClNO_2$ photolysis is a significant source of Cl atoms in the early morning, and other sources such as the photolysis of Cl_2, $ClONO_2$, HCl, ICl, and BrCl by sunlight can also contribute to Cl atom concentrations later in the day (Peng et al., 2020). Besides, some Cl-OOMs could be formed through secondary reactions involving OH radicals with Cl-VOCs or intermediates, rather than direct Cl atom-initiated reaction. While distinguishing these pathways is beyond the scope of this study, the formation of Cl-OOMs is likely influenced by both Cl- and OH-initiated mechanisms under ambient conditions, especially in the presence of NO_X.

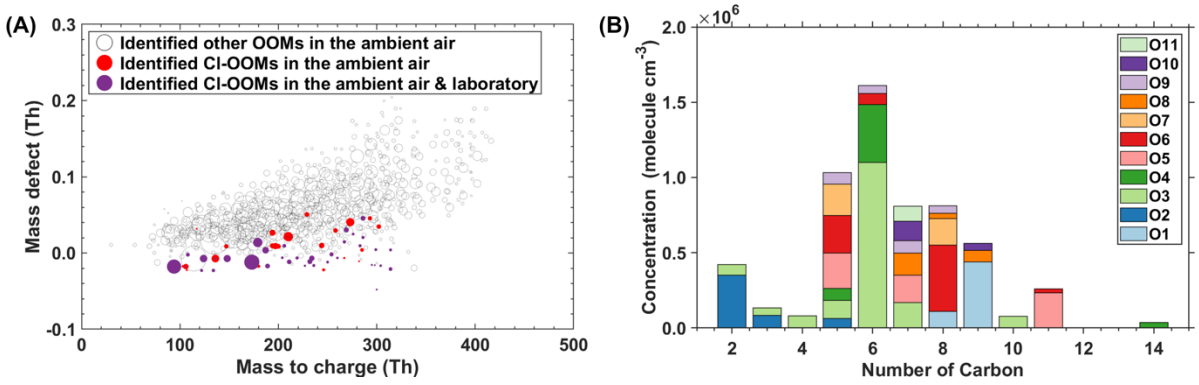

Figure 4. (A). Mass defect plot of detected OOMs by a nitrate-CI-APi-LToF in ambient air in suburban Shanghai. Cl-OOMs only observed in the ambient atmosphere were marked in red, and Cl-OOMs observed in both ambient and lab were marked in purple. The size of the circle is proportional to the concentration of compounds in the ambient. (B). Distribution of carbon and oxygen number of gas-phase Cl-OOMs identified in suburban Shanghai. The color codes correspond to the number of oxygen atoms.

3.5. Health effect of ambient Cl-OOMs.

Table S5 presents a detailed toxicity estimation of various Cl-OOMs, including $C_7H_7N_2ClO_9$, $C_8H_{10}NClO_7$, and $C_9H_{15}ClO_8$, which were identified in the suburban Shanghai atmosphere and laboratory experiments. These estimations are based on the potential chemical structures of these Cl-OOMs. We characterized the toxicity of these Cl-OOMs using persistence, bioaccumulative and toxic (PBT) criteria, as outlined in Table S5. Additionally, we conducted a comparative analysis of their toxicity relative to that of naphthalene, a compound whose atmospheric toxicity has been extensively studied.

Compounds with short OH radical reaction half-lives and bioconcentration factors (BCF) are unlikely to be persistent and bioaccumulative. Among these Cl-OOMs, $C_8H_{10}NClO_7$ (II) exhibits the slowest degradation rate with OH radicals with a half-life of 5 days, which suggests that it is a potential new persistent pollutant (half-life > 2 days) in the atmosphere (Europe, 2023).

As indicated by the pLD_{50} values, toxicity levels of most Cl-OOMs are lower than that of naphthalene, except for $C_8H_{10}NClO_8$, $C_8H_{10}NClO_7$ (I), and $C_7H_7N_2ClO_8$ (Table S5). Among these compounds, $C_8H_{10}NClO_7$ (I) is identified with the highest predicted toxicity, followed by compound $C_8H_{10}NClO_8$. The pLD_{50} of these compounds is categorized within level 3, signifying their potential for a considerable acute toxicity.

Notably, the pLD_{50} values of Cl-OOMs are found to be akin to those of naphthalene. However, given that their concentration in suburban Shanghai (0.55 ppt) is merely one percent of that of naphthalene (50 ppt) as measured in this study, the total probabilistic hazard quotient (PrHQ, defined as the product of estimated human exposure (ambient concentration) and pLD_{50} in this study) of Cl-OOMs is lower. Despite this lower PrHQ, it is important to recognize that each of the evaluated Cl-OOMs may pose risks of developmental toxicity and mutagenicity, which underscores the need for a thorough understanding of the toxicological implications of Cl-OOMs in the atmosphere.

4. Conclusions

In summary, this study highlights the Cl-addition-initiated reaction as a non-negligible pathway in the reaction of Cl atoms with aromatics. Field measurements in suburban Shanghai revealed 51 gaseous Cl-OOM species, with 38 of these Cl-OOMs also detected in our laboratory experiments. This suggests that these Cl-OOMs likely derive from reactions between Cl atoms and aromatics. Considering the significant role of Cl atoms in daily atmospheric oxidation processes, overlooking the Cl-addition pathway could lead to ignoring the formation of Cl-OOMs from aromatic compounds in the atmosphere. This study, therefore, highlights the necessity of incorporating both pathways in the models for a more accurate assessment of the

atmospheric fate of Cl atoms and aromatics in urban settings. In addition, health effect evaluation indicates that all assessed Cl-OOMs may possess developmental toxicity, and nearly half of the compounds may exhibit carcinogenic effects. Considering the critical role of aromatics in the urban air and recent observations reporting increased levels of reactive chlorine species in polluted atmospheres, our study offers timely insights into the chemical processes between Cl atoms and aromatics occurring in anthropogenically influenced atmospheres and the adverse health effects of these Cl-containing reaction products.

Data availability.

The data used in this study are available upon request from Lei Yao (lei_yao@fudan.edu.cn) and Lin Wang (lin_wang@fudan.edu.cn).

Author contributions.

LY and LW conceived and designed this study and revised the manuscript. CL analyzed and interpreted data, drafted and revised the manuscript. CL and YW contributed to the modeling of the data. MF and XC contributed to the health effect analysis.

Competing interests.

The contact author has declared that none of the authors has any competing interests.

Financial support. This research was supported by the National Key Research and Development Program of China (2022YFC3704100) and the National Natural Science Foundation of China (22376031, 21925601, 92143301).

References

Alage, S., Michoud, V., Harb, S., Picquet-Varrault, B., Cirtog, M., Kumar, A., Rissanen, M., and Cantrell, C.: A nitrate ion chemical-ionization atmospheric-pressure-interface time-of-flight mass spectrometer (NO3- ToFCIMS) sensitivity study, Atmos. Meas. Tech., 17, 4709–4724, https://doi.org/10.5194/amt-17-4709-2024, 2024.

Berndt, T., Scholz, W., Mentler, B., Fischer, L., Herrmann, H., Kulmala, M., and Hansel, A.: Accretion Product Formation from Self- and Cross-Reactions of RO2 Radicals in the Atmosphere., Angewandte Chemie Int Ed Engl, 57, 3820–3824, https://doi.org/10.1002/anie.201710989, 2017.

Bhattacharyya, N., Modi, M., Jahn, L. G., and Ruiz, L. H.: Different chlorine and hydroxyl radical environments impact m -xylene oxidation products, Environ. Sci.: Atmos., https://doi.org/10.1039/d3ea00024a, 2023.

Bianchi, F., Kurtén, T., Riva, M., Mohr, C., Rissanen, M. P., Roldin, P., Berndt, T., Crounse, J. D., Wennberg, P. O., Mentel, T. F., Wildt, J., Junninen, H., Jokinen, T., Kulmala, M., Worsnop, D. R., Thornton, J. A., Donahue, N., Kjaergaard, H. G., and Ehn, M.: Highly Oxygenated Organic Molecules (HOM) from Gas-Phase Autoxidation Involving Peroxy Radicals: A Key Contributor to Atmospheric Aerosol, Chem Rev, 119, 3472–3509, https://doi.org/10.1021/acs.chemrev.8b00395, 2019.

Breton, M. L., Hallquist, Å. M., Pathak, R. K., Simpson, D., Wang, Y., Johansson, J., Zheng, J., Yang, Y., Shang, D., Wang, H., Liu, Q., Chan, C., Wang, T., Bannan, T. J., Priestley, M., Percival, C. J., Shallcross, D. E., Lu, K., Guo, S., Hu, M., and Hallquist, M.: Chlorine oxidation of VOCs at a semi-rural site in Beijing: significant chlorine liberation from ClNO2 and subsequent gas- and particle-phase Cl–VOC production, Atmos Chem Phys, 18, 13013–13030, https://doi.org/10.5194/acp-18-13013-2018, 2018.

Cai, X., Ziemba, L. D., and Griffin, R. J.: Secondary aerosol formation from the oxidation of toluene by chlorine atoms, Atmos Environ, 42, 7348–7359, https://doi.org/10.1016/j.atmosenv.2008.07.014, 2008.

Chang, C.-T., Liu, T.-H., and Jeng, F.-T.: Atmospheric concentrations of the Cl atom, ClO radical, and HO radical in the coastal marine boundary layer, Environ. Res., 94, 67–74, https://doi.org/10.1016/j.envres.2003.07.008, 2004.

Chen, M., Yin, M., Su, Y., Li, R., Liu, K., Wu, Z., and Weng, X.: Atmospheric heterogeneous reaction of chlorobenzene on mineral α-Fe2O3 particulates: a chamber experiment study, Front. Environ. Sci. Eng., 17, 134, https://doi.org/10.1007/s11783-023-1734-9, 2023.

572 Cubison, M. J. and Jimenez, J. L.: Statistical precision of the intensities retrieved from
573 constrained fitting of overlapping peaks in high-resolution mass spectra, Atmos. Meas. Tech.,
574 8, 2333–2345, https://doi.org/10.5194/amt-8-2333-2015, 2015.

575 DeMore, W. B., Sander, N. P., Golden, D. M., Hampson, R. F., Kurylo, M. J., Howard, C. J.,
576 Ravishankara, A. R., Kolb, C. E., and Molina, M. J.: Chemical Kinetics and Photochemical
577 Data for Use in Stratospheric Modeling, JPL Publication, 1997.

578 Ehn, M., Junninen, H., Petäjä, T., Kurtén, T., Kerminen, V.-M., Schobesberger, S., Manninen,
579 H. E., Ortega, I. K., Vehkamäki, H., Kulmala, M., and Worsnop, D. R.: Composition and
580 temporal behavior of ambient ions in the boreal forest, Atmos. Chem. Phys., 10, 8513–8530,
581 https://doi.org/10.5194/acp-10-8513-2010, 2010.

582 Ehn, M., Thornton, J. A., Kleist, E., Sipilä, M., Junninen, H., Pullinen, I., Springer, M., Rubach,
583 F., Tillmann, R., Lee, B., Lopez-Hilfiker, F., Andres, S., Acir, I.-H., Rissanen, M., Jokinen, T.,
584 Schobesberger, S., Kangasluoma, J., Kontkanen, J., Nieminen, T., Kurtén, T., Nielsen, L. B.,
585 Jørgensen, S., Kjaergaard, H. G., Canagaratna, M., Maso, M. D., Berndt, T., Petäjä, T., Wahner,
586 A., Kerminen, V.-M., Kulmala, M., Worsnop, D. R., Wildt, J., and Mentel, T. F.: A large source
587 of low-volatility secondary organic aerosol, Nature, 506, 476–479,
588 https://doi.org/10.1038/nature13032, 2014.

589 Eisele, F. L. and Tanner, D. J.: Measurement of the gas phase concentration of H2SO4 and
590 methane sulfonic acid and estimates of H2SO4 production and loss in the atmosphere, J
591 Geophys Res Atmospheres, 98, 9001–9010, https://doi.org/10.1029/93jd00031, 1993.

592 Europe, U. N. E. C. for: Globally Harmonized System of Classification and Labelling of
593 Chemicals (GHS), Glob. Harmon. Syst. Classif. Label. Chem. (GHS),
594 https://doi.org/10.18356/9789210019071, 2023.

595 Finlayson-Pitts, B. J., Keoshian, C. J., Buehler, B., and Ezell, A. A.: Kinetics of reaction of
596 chlorine atoms with some biogenic organics, Int J Chem Kinet, 31, 491–499,
597 https://doi.org/10.1002/(sici)1097-4601(1999)31:7<491::aid-kin4>3.0.co;2-e, 1999.

598 Heinritzi, M., Simon, M., Steiner, G., Wagner, A. C., Kürten, A., Hansel, A., and Curtius, J.:
599 Characterization of the mass-dependent transmission efficiency of a CIMS, Atmos Meas Tech,
600 9, 1449–1460, https://doi.org/10.5194/amt-9-1449-2016, 2016.

601 Henschler, D.: Toxicity of Chlorinated Organic Compounds: Effects of the Introduction of
602 Chlorine in Organic Molecules, Angewandte Chemie Int Ed Engl, 33, 1920–1935,
603 https://doi.org/10.1002/anie.199419201, 1994.

Huang, M., Wang, Z., Hao, L., and Zhang, W.: DFT study on the abstraction and addition of Cl atom with toluene, Comput. Theor. Chem., 996, 44–50, https://doi.org/10.1016/j.comptc.2012.07.011, 2012.

Huang, Y., Zhao, R., Charan, S. M., Kenseth, C. M., Zhang, X., and Seinfeld, J. H.: Unified Theory of Vapor–Wall Mass Transport in Teflon-Walled Environmental Chambers, Environ. Sci. Technol., 52, 2134–2142, https://doi.org/10.1021/acs.est.7b05575, 2018.

Jahn, L. G., McPherson, K. N., and Ruiz, L. H.: Effects of Relative Humidity and Photoaging on the Formation, Composition, and Aging of Ethylbenzene SOA: Insights from Chamber Experiments on Chlorine Radical-Initiated Oxidation of Ethylbenzene, ACS Earth Space Chem., 8, 675–688, https://doi.org/10.1021/acsearthspacechem.3c00279, 2024.

Keene, William. C., Khalil, M. A. K., Erickson, David. J., McCulloch, A., Graedel, T. E., Lobert, J. M., Aucott, M. L., Gong, S. L., Harper, D. B., Kleiman, G., Midgley, P., Moore, R. M., Seuzaret, C., Sturges, W. T., Benkovitz, C. M., Koropalov, V., Barrie, L. A., and Li, Y. F.: Composite global emissions of reactive chlorine from anthropogenic and natural sources: Reactive Chlorine Emissions Inventory, J. Geophys. Res.: Atmos., 104, 8429–8440, https://doi.org/10.1029/1998jd100084, 1999.

Knipping, E. M., Lakin, M. J., Foster, K. L., Jungwirth, P., Tobias, D. J., Gerber, R. B., Dabdub, D., and Finlayson-Pitts, B. J.: Experiments and Simulations of Ion-Enhanced Interfacial Chemistry on Aqueous NaCl Aerosols, Science, 288, 301–306, https://doi.org/10.1126/science.288.5464.301, 2000.

Krechmer, J., Lopez-Hilfiker, F., Koss, A., Hutterli, M., Stoermer, C., Deming, B., Kimmel, J., Warneke, C., Holzinger, R., Jayne, J., Worsnop, D., Fuhrer, K., Gonin, M., and Gouw, J. de: Evaluation of a New Reagent-Ion Source and Focusing Ion–Molecule Reactor for Use in Proton-Transfer-Reaction Mass Spectrometry, Anal Chem, 90, 12011–12018, https://doi.org/10.1021/acs.analchem.8b02641, 2018.

Kulmala, M., Kontkanen, J., Junninen, H., Lehtipalo, K., Manninen, H. E., Nieminen, T., Petäjä, T., Sipilä, M., Schobesberger, S., Rantala, P., Franchin, A., Jokinen, T., Järvinen, E., Äijälä, M., Kangasluoma, J., Hakala, J., Aalto, P. P., Paasonen, P., Mikkilä, J., Vanhanen, J., Aalto, J., Hakola, H., Makkonen, U., Ruuskanen, T., Mauldin, R. L., Duplissy, J., Vehkamäki, H., Bäck, J., Kortelainen, A., Riipinen, I., Kurtén, T., Johnston, M. V., Smith, J. N., Ehn, M., Mentel, T. F., Lehtinen, K. E. J., Laaksonen, A., Kerminen, V.-M., and Worsnop, D. R.: Direct Observations of Atmospheric Aerosol Nucleation, Science, 339, 943–946, https://doi.org/10.1126/science.1227385, 2013.

Kürten, A., Rondo, L., Ehrhart, S., and Curtius, J.: Performance of a corona ion source for measurement of sulfuric acid by chemical ionization mass spectrometry, Atmos Meas Tech, 4, 437–443, https://doi.org/10.5194/amt-4-437-2011, 2011.

Kürten, A., Rondo, L., Ehrhart, S., and Curtius, J.: Calibration of a Chemical Ionization Mass Spectrometer for the Measurement of Gaseous Sulfuric Acid, J Phys Chem, 116, 6375–6386, https://doi.org/10.1021/jp212123n, 2012.

Kürten, A., Bergen, A., Heinritzi, M., Leiminger, M., Lorenz, V., Piel, F., Simon, M., Sitals, R., Wagner, A. C., and Curtius, J.: Observation of new particle formation and measurement of sulfuric acid, ammonia, amines and highly oxidized organic molecules at a rural site in central Germany, Atmos Chem Phys, 16, 12793–12813, https://doi.org/10.5194/acp-16-12793-2016, 2016.

Liu, X., Qu, H., Huey, L. G., Wang, Y., Sjostedt, S., Zeng, L., Lu, K., Wu, Y., Hu, M., Shao, M., Zhu, T., and Zhang, Y.: High Levels of Daytime Molecular Chlorine and Nitryl Chloride at a Rural Site on the North China Plain, Environ Sci Technol, 51, 9588–9595, https://doi.org/10.1021/acs.est.7b03039, 2017.

Lu, Y., Liu, L., Ning, A., Yang, G., Liu, Y., Kurtén, T., Vehkamäki, H., Zhang, X., and Wang, L.: Atmospheric Sulfuric Acid-Dimethylamine Nucleation Enhanced by Trifluoroacetic Acid, Geophys Res Lett, 47, https://doi.org/10.1029/2019gl085627, 2020.

Ma, W., Chen, X., Xia, M., Liu, Y., Wang, Y., Zhang, Y., Zheng, F., Zhan, J., Hua, C., Wang, Z., Wang, W., Fu, P., Kulmala, M., and Liu, Y.: Reactive Chlorine Species Advancing the Atmospheric Oxidation Capacities of Inland Urban Environments, Environ. Sci. Technol., 57, 14638–14647, https://doi.org/10.1021/acs.est.3c05169, 2023.

Molteni, U., Bianchi, F., Klein, F., Haddad, I. E., Frege, C., Rossi, M. J., Dommen, J., and Baltensperger, U.: Formation of highly oxygenated organic molecules from aromatic compounds, Atmos Chem Phys, 18, 1909–1921, https://doi.org/10.5194/acp-18-1909-2018, 2018.

Orlando, J. J., Tyndall, G. S., Apel, E. C., Riemer, D. D., and Paulson, S. E.: Rate coefficients and mechanisms of the reaction of cl-atoms with a series of unsaturated hydrocarbons under atmospheric conditions, Int. J. Chem. Kinet., 35, 334–353, https://doi.org/10.1002/kin.10135, 2003.

Peng, X., Wang, W., Xia, M., Chen, H., Ravishankara, A. R., Li, Q., Saiz-Lopez, A., Liu, P., Zhang, F., Zhang, C., Xue, L., Wang, X., George, C., Wang, J., Mu, Y., Chen, J., and Wang, T.: An unexpected large continental source of reactive bromine and chlorine with significant impact on wintertime air quality, Natl. Sci. Rev., 8, nwaa304, https://doi.org/10.1093/nsr/nwaa304, 2020.

Peng, X., Wang, T., Wang, W., Ravishankara, A. R., George, C., Xia, M., Cai, M., Li, Q., Salvador, C. M., Lau, C., Lyu, X., Poon, C. N., Mellouki, A., Mu, Y., Hallquist, M., Saiz-Lopez, A., Guo, H., Herrmann, H., Yu, C., Dai, J., Wang, Y., Wang, X., Yu, A., Leung, K., Lee, S.,

675 and Chen, J.: Photodissociation of particulate nitrate as a source of daytime tropospheric Cl2,
676 Nat Commun, 13, 939, https://doi.org/10.1038/s41467-022-28383-9, 2022.

677 Priestley, M., Breton, M. le, Bannan, T. J., Worrall, S. D., Bacak, A., Smedley, A. R. D., Reyes-
678 Villegas, E., Mehra, A., Allan, J., Webb, A. R., Shallcross, D. E., Coe, H., and Percival, C. J.:
679 Observations of organic and inorganic chlorinated compounds and their contribution to chlorine
680 radical concentrations in an urban environment in northern Europe during the wintertime,
681 Atmos Chem Phys, 18, 13481–13493, https://doi.org/10.5194/acp-18-13481-2018, 2018.

682 Ragains, M. L. and Finlayson-Pitts, B. J.: Kinetics and Mechanism of the Reaction of Cl Atoms
683 with 2-Methyl-1,3-butadiene (Isoprene) at 298 K, J. Phys. Chem. A, 101, 1509–1517,
684 https://doi.org/10.1021/jp962786m, 1997.

685 Riva, M., Healy, R. M., Flaud, P.-M., Perraudin, E., Wenger, J. C., and Villenave, E.: Gas- and
686 Particle-Phase Products from the Chlorine-Initiated Oxidation of Polycyclic Aromatic
687 Hydrocarbons., J Phys Chem, 119, 11170–81, https://doi.org/10.1021/acs.jpca.5b04610, 2015.

688 Shang, D., Peng, J., Guo, S., Wu, Z., and Hu, M.: Secondary aerosol formation in winter haze
689 over the Beijing-Tianjin-Hebei Region, China, Front. Environ. Sci. Eng., 15, 34,
690 https://doi.org/10.1007/s11783-020-1326-x, 2021.

691 Shi, J. and Bernhard, M. J.: Kinetic studies of Cl-atom reactions with selected aromatic
692 compounds using the photochemical reactor-FTIR spectroscopy technique, Int. J. Chem. Kinet.,
693 29, 349–358, https://doi.org/10.1002/(sici)1097-4601(1997)29:5<349::aid-kin5>3.0.co;2-u,
694 1997.

695 Sokolov, O., Hurley, M. D., Wallington, T. J., Kaiser, E. W., Platz, J., Nielsen, O. J., Berho, F.,
696 Rayez, M.-T., and Lesclaux, R.: Kinetics and Mechanism of the Gas-Phase Reaction of Cl
697 Atoms with Benzene, J. Phys. Chem. A, 102, 10671–10681, https://doi.org/10.1021/jp9828080,
698 1998.

699 Tham, Y. J., Wang, Z., Li, Q., Yun, H., Wang, W., Wang, X., Xue, L., Lu, K., Ma, N., Bohn,
700 B., Li, X., Kecorius, S., Größ, J., Shao, M., Wiedensohler, A., Zhang, Y., and Wang, T.:
701 Significant concentrations of nitryl chloride sustained in the morning: investigations of the
702 causes and impacts on ozone production in a polluted region of northern China, Atmos Chem
703 Phys, 16, 14959–14977, https://doi.org/10.5194/acp-16-14959-2016, 2016.

704 Thornton, J. A., Kercher, J. P., Riedel, T. P., Wagner, N. L., Cozic, J., Holloway, J. S., Dubé,
705 W. P., Wolfe, G. M., Quinn, P. K., Middlebrook, A. M., Alexander, B., and Brown, S. S.: A
706 large atomic chlorine source inferred from mid-continental reactive nitrogen chemistry, Nature,
707 464, 271–274, https://doi.org/10.1038/nature08905, 2010.

UN: Globally Harmonized System of Classification and Labelling of Chemicals (GHS), Glob. Harmon. Syst. Classif. Label. Chem. (GHS), https://doi.org/10.18356/9789210019071, 2023.

Vereecken, L. and Nozière, B.: H migration in peroxy radicals under atmospheric conditions, Atmos. Chem. Phys., 20, 7429–7458, https://doi.org/10.5194/acp-20-7429-2020, 2020.

Wang, C., Collins, D. B., and Abbatt, J. P. D.: Indoor Illumination of Terpenes and Bleach Emissions Leads to Particle Formation and Growth, Environ. Sci. Technol., 53, 11792–11800, https://doi.org/10.1021/acs.est.9b04261, 2019.

Wang, C., Liggio, J., Wentzell, J. J. B., Jorga, S., Folkerson, A., and Abbatt, J. P. D.: Chloramines as an important photochemical source of chlorine atoms in the urban atmosphere, Proc. Natl. Acad. Sci., 120, e2220889120, https://doi.org/10.1073/pnas.2220889120, 2023.

Wang, D. S. and Ruiz, L. H.: Secondary organic aerosol from chlorine-initiated oxidation of isoprene, Atmos Chem Phys, 17, 13491–13508, https://doi.org/10.5194/acp-17-13491-2017, 2017.

Wang, D. S., Masoud, C. G., Modi, M., and Ruiz, L. H.: Isoprene-Chlorine Oxidation in the Presence of NOx and Implications for Urban Atmospheric Chemistry., Environ Sci Technol, https://doi.org/10.1021/acs.est.1c07048, 2022.

Wang, L., Arey, J., and Atkinson, R.: Reactions of Chlorine Atoms with a Series of Aromatic Hydrocarbons, Environ Sci Technol, 39, 5302–5310, https://doi.org/10.1021/es0479437, 2005.

Wang, M., Yang, L., Liu, X., Wang, Z., Liu, G., and Zheng, M.: Hexachlorobutadiene emissions from typical chemical plants, Front. Environ. Sci. Eng., 15, 60, https://doi.org/10.1007/s11783-020-1352-8, 2021.

Wang, S., Wu, R., Berndt, T., Ehn, M., and Wang, L.: Formation of Highly Oxidized Radicals and Multifunctional Products from the Atmospheric Oxidation of Alkylbenzenes, Environ. Sci. Technol., 51, 8442–8449, https://doi.org/10.1021/acs.est.7b02374, 2017.

Wang, Y., Riva, M., Xie, H., Heikkinen, L., Schallhart, S., Zha, Q., Yan, C., He, X.-C., Peräkylä, O., and Ehn, M.: Formation of highly oxygenated organic molecules from chlorine-atom-initiated oxidation of alpha-pinene, Atmos Chem Phys, 20, 5145–5155, https://doi.org/10.5194/acp-20-5145-2020, 2020.

Wang, Y., Li, C., Zhang, Y., Li, Y., Yang, G., Yang, X., Wu, Y., Yao, L., Zhang, H., and Wang, L.: Secondary reactions of aromatics-derived oxygenated organic molecules lead to plentiful highly oxygenated organic molecules within an intraday OH exposure, Atmos. Chem. Phys., 24, 7961–7981, https://doi.org/10.5194/acp-24-7961-2024, 2024.

Wingenter, O. W., Sive, B. C., Blake, N. J., Blake, D. R., and Rowland, F. S.: Atomic chlorine concentrations derived from ethane and hydroxyl measurements over the equatorial Pacific Ocean: Implication for dimethyl sulfide and bromine monoxide, J. Geophys. Res.: Atmos., 110, https://doi.org/10.1029/2005jd005875, 2005.

Wu, Y., Huo, J., Yang, G., Wang, Y., Wang, L., Wu, S., Yao, L., Fu, Q., and Wang, L.: Measurement report: Production and loss of atmospheric formaldehyde at a suburban site of Shanghai in summertime, Atmos. Chem. Phys., 23, 2997–3014, https://doi.org/10.5194/acp-23-2997-2023, 2023.

Xu, L., Møller, K. H., Crounse, J. D., Kjaergaard, H. G., and Wennberg, P. O.: New Insights into the Radical Chemistry and Product Distribution in the OH-Initiated Oxidation of Benzene, Environ. Sci. Technol., 54, 13467–13477, https://doi.org/10.1021/acs.est.0c04780, 2020.

Yang, G., Huo, J., Wang, L., Wang, Y., Wu, S., Yao, L., Fu, Q., and Wang, L.: Total OH Reactivity Measurements in a Suburban Site of Shanghai, J Geophys Res Atmospheres, 127, https://doi.org/10.1029/2021jd035981, 2022.

Yang, X., Ren, S., Wang, Y., Yang, G., Li, Y., Li, C., Wang, L., Yao, L., and Wang, L.: Volatility Parametrization of Low-Volatile Components of Ambient Organic Aerosols Based on Molecular Formulas, Environ. Sci. Technol., https://doi.org/10.1021/acs.est.3c02073, 2023.

Zhang, M., Chen, S., Yu, X., Vikesland, P., and Pruden, A.: Degradation of extracellular genomic, plasmid DNA and specific antibiotic resistance genes by chlorination, Front. Environ. Sci. Eng., 13, 38, https://doi.org/10.1007/s11783-019-1124-5, 2019.

Zhao, Y., Thornton, J. A., and Pye, H. O. T.: Quantitative constraints on autoxidation and dimer formation from direct probing of monoterpene-derived peroxy radical chemistry, Proc National Acad Sci, 115, 12142–12147, https://doi.org/10.1073/pnas.1812147115, 2018.